JOURNAL OF SOLID STATE CHEMISTRY 117, 1–7 (1995)

Synthesis and Thermal Stability of $LiCoO_2$

Ermete Antolini* and Maurizio Ferretti†

*Ansaldo Ricerche s.r.l., Corso Perrone 25, 16161 Genoa, Italy; and †Istituto di Chimica Fisica, Università di Genova, Corso Europa 26, 16132 Genoa, Italy

Received January 7, 1994; in revised form August 24, 1994; accepted September 1, 1994

Lithium cobalt oxide, $LiCoO_2$, was synthesized in air from a mixture of metallic cobalt and lithium carbonate powder and annealed at 850 to 1100°C to evaluate its thermal stability. Single-phase $LiCoO_2$ was thermally stable at 850°C. The weight loss of samples at temperatures higher than 850°C and the presence of Co_3O_4 in the X-ray diffraction pattern at $T > 900$°C indicated the decomposition of $LiCoO_2$. The time dependence of lithium oxide evaporation from $LiCoO_2$ indicated that at 900°C the decomposition kinetics is controlled by $LiCoO_2$ decomposition, while at $T > 900$°C the process is controlled by the diffusion of lithium ions in nonstoichiometric lithium cobalt oxide, $Li_yCo_{2-y}O_2$, and in the CoO solid phase surrounding the particles. At $T > 1000$°C the formation of $Li_xCo_{1-x}O$ solid solution was also noted. Moreover, the decomposition rate seemed to depend on the temperature during the formation of lithium cobalt oxide.

INTRODUCTION

Lithium cobalt oxide, $LiCoO_2$, is a compound with a layered rock-salt structure in which the Li^+ and Co^{3+} ions are situated in alternate planes (111) of the cubic rock-salt structure (1, 2). This (111) ordering introduces a slight distortion of the lattice to hexagonal symmetry. Hence, $LiCoO_2$ crystallizes in the space group $R3m$ with cell constants $a = 2.816$ Å and $c = 14.08$ Å (3). $LiCoO_2$ is used as a cathode material in advanced rechargeable lithium batteries (3, 4) and shows promise as a replacement for NiO as the cathode material in molten carbonate fuel cells (5, 6).

$LiCoO_2$ has been prepared using as cobalt compounds Co_3O_4 (7) or Co^{2+} salts, $CoCO_3$ (8, 9) and $Co(NO_3)_2$ (10), both at high temperature (800–900°C) (2, 8) and at low temperature (400°C) (11).

This work deals with the synthesis of $LiCoO_2$ starting from Co metallic powder and Li_2CO_3 and with the evaluation of its thermal stability. Nonstoichiometric layered $LiCoO_2$ is designated $LiyCO_{2-y}O_2$. The cubic (disordered) rock-salt structure is designated $Li_xCo_{1-x}O$.

EXPERIMENTAL

Green Preparation

Cobalt powder (Matthey Reagent, 99.8%) of size 1.6 μm and lithium carbonate (Merck, 5671) were used as starting materials. The Li/Co atomic ratios were 1.14 : 1 (method A) and 1.09 : 1 (method B), higher than the stoichiometric ratio of 1 : 1 to offset lithium loss by Li_2O evaporation during $LiCoO_2$ synthesis. These powders were ball milled in deionized water with a binder (methylcellulose, Methocel MC, Fluka Chemie 64620) and an antifoam agent (polydimethylsiloxane and silica, Antifoam A, Dow Corning Corp.) to get a viscous slurry. Two methods were used to obtain this slurry:

Method A: The Co and Li_2CO_3 powders were put in deionized water together with the binder and the antifoam agent and were ball milled for 24 hr.

Method B: First, a solution of the binder and the antifoam agent was prepared. Then, the Co and Li_2CO_3 powders were added to the solution of the binder and ball milled for 24 hr. In our experience the separation from the reaction mixture of a film of lithium carbonate in the vessel was not observed.

After milling, the resulting slurries were degassed and then cast onto a bees wax-coated glass surface. After drying, the tape was cut in the form of disk samples (diameter, 5 cm) and submitted to thermal treatment.

Thermal Treatment

Thermal treatments were performed in air with a BICASA BE 35 furnace. Thermogravimetric measurements were performed with a Netsch STA 409 simultaneous thermal analyzer. The container material for the thermal treatment (TGA and furnace) was high-purity Al_2O_3 and no trace of reaction between the container and the samples was noted. Measurements were performed in air on crushed samples of similar mass. For both thermal treatment in the furnace and thermogravimetric analysis, each measurement consisted of three steps:

0022-4596/95 $6.00

(a) a dynamic step during which the samples were heated from room temperature to temperatures around 850, 900, 950, 1000, and 1100°C at a rate of 3°C/min;

(b) an isothermal step during which the samples were maintained for 5 hr at the maximum temperature reached during the first step;

(c) a dynamic step during which the samples were cooled from the maximum temperature to room temperature at a rate of 4°C/min.

Thermal treatments in the furnace were performed at all stated temperatures on tapes from both method A (green A) and method B (green B). Thermogravimetric analysis was performed at all temperatures on green A, but only at 950°C on green B.

Pure Co powder was subjected to thermogravimetric analysis by a dynamic step at room temperature to 950°C at a rate of 3°C/min, to compare it with Co/Li_2CO_3 mixtures.

Diffractometric Measurements

Following thermal treatment in the furnace, the samples were submitted to X-ray diffraction measurements. Diffraction data were obtained with a Philips PW1729 powder diffractometer equipped with a Philips PW1771 vertical goniometer using filtered Cu$K\alpha$ radiation.

RESULTS AND DISCUSSION

Green A was nonhomogeneous through its thickness: the presence of two layers of different composition, one Li_2CO_3-rich, the other Li_2CO_3-poor, was noted. The density of green A was 0.92 g/cm^3. Green B was homogeneous and had a density of 1.20 g/cm^3.

Figure 1 shows the densities of samples from green A and green B as a function of temperature following thermal treatment in a furnace. For both samples the density slowly increased with increasing temperature up to 1050°C, while an even greater increase in density was revealed at 1100°C.

Synthesis

The formation of single-phase lithium cobalt oxide at 850°C was revealed by X-ray diffraction patterns following thermal treatment in a furnace of samples from green A (Fig. 2) and green B (Fig. 3).

Table 1 shows weight loss Dm/m_g (where Dm is the mass change of the sample following thermal treatment and m_g is the mass of the sample before thermal treatment) following thermal treatment in a furnace for green A and green B; the calculated weight loss $(Dm/m_g)_{calc}$ was obtained by considering complete binder burnout, Li_2CO_3 decomposition, $LiCoO_2$ formation, and excess Li_2O evaporation. As can be seen in Table 1 at 850°C, the calculated and experimental weight losses for green A, were in good agreement, while for green B the experimental weight loss was higher than the calculated value. So, on the basis of weight variation, in the case of green A, stoichiometric $LiCoO_2$ was formed, while in the case

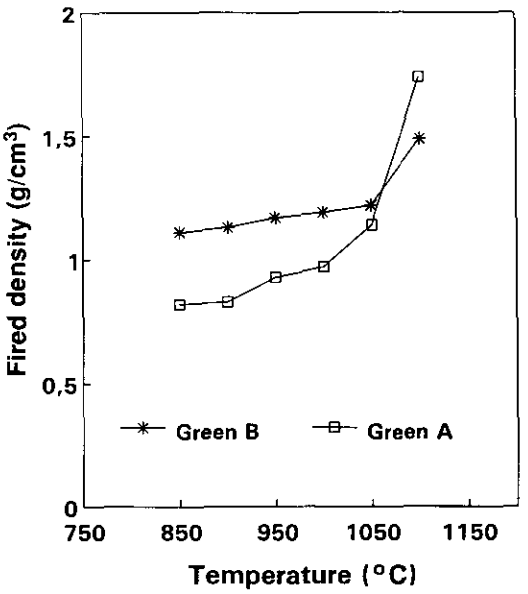

FIG. 1. Dependence on thermal treatment temperature of the density of samples from green A and green B.

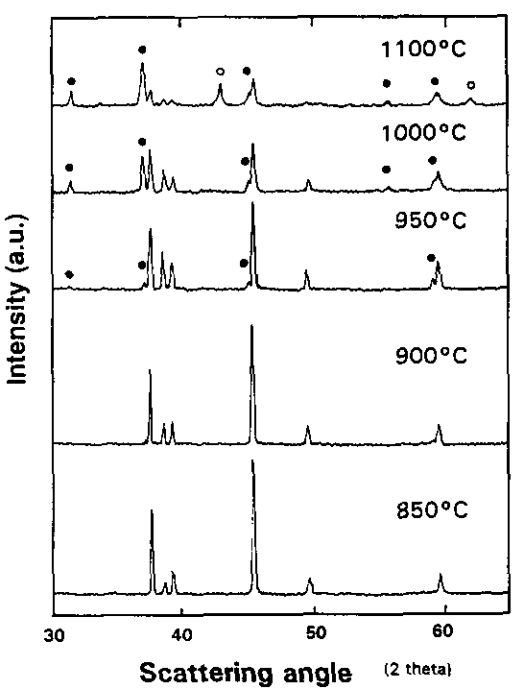

FIG. 2. X-ray diffraction patterns of samples from green A following thermal treatment in furnace in the temperature range 850–1100°C: (●) Co_3O_4, (○) $Li_xCo_{1-x}O$.

TABLE 1

Calculated and Experimental Weight Loss of Samples from Green A and Green B following Thermal Treatment in Furnace in the Temperature Range 850–1100°C

Green A $(Dm/m_g)_{calc}$ = 15.3%				Green B $(Dm/m_g)_{calc}$ = 12.6%			
Temperature (°C)	m_g (g)	m_s (g)	Dm/m_g (%)	Temperature (°C)	m_g (g)	m_s (g)	Dm/m_g (%)
850	0.422	0.357	15.4	850	1.031	0.883	14.4
900	0.373	0.314	15.8	900	1.010	0.858	15.0
950	0.387	0.323	16.5	950	1.035	0.855	17.4
1000	0.386	0.303	21.5	1000	1.045	0.823	21.2
1100	0.492	0.352	28.5	1100	1.019	0.745	26.9

Note. m_g and m_s are the experimental weights of green tapes and sintered samples, respectively. The measurement error is ±0.0005 g.

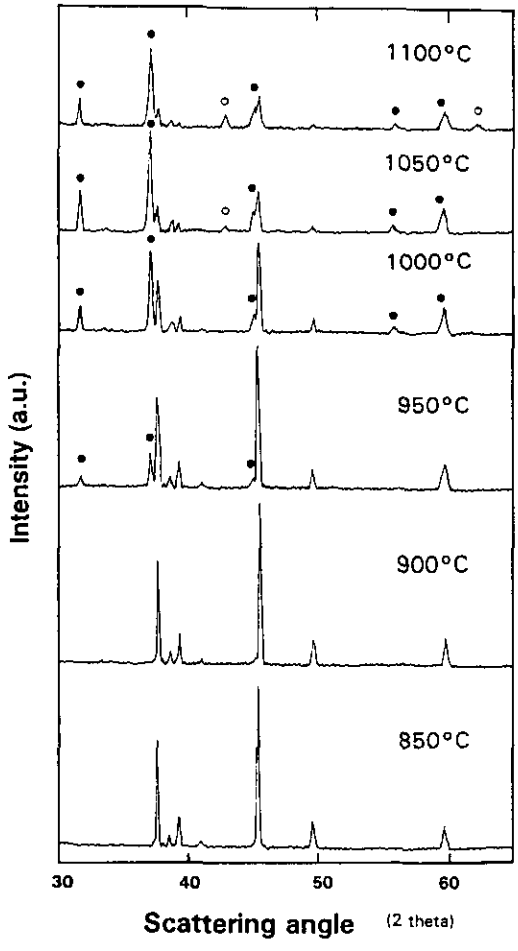

FIG. 3. X-ray diffraction patterns of samples from green B following thermal treatment in furnace in the temperature range 850–1100°C: (●) Co_3O_4, (○) $Li_xCo_{1-x}O$.

of green B, ascribing the differences between experimental and calculated weight loss to lithium oxide evaporation, nonstoichiometric $Li_yCo_{2-y}O_2$ was formed.

Table 2 shows a and c parameters of the hexagonal cell of $LiCoO_2$; at all temperatures the a parameter (intralayer metal–metal distance) decreased and the c parameter (interslab distance) increased going from $LiCoO_2$ from green A to $LiCoO_2$ from green B.

Figures 4a–4c show thermogravimetric measurements (dynamic step) performed on pure Co, green A, and green B, respectively. The curve of pure Co increased monotonically from 260 to 660°C by cobalt oxidation to Co_3O_4; then, starting from 895°C, the weight decrease indicated the transition from Co_3O_4 to CoO. The curves of green A and green B, after the initial weight decrease by organic burnout, went through a maximum at T_{max} = 547°C (green A) and 523°C (green B). This result suggests that $LiCoO_2$ formation took place in the following way:

—oxidation of Co to form Co_3O_4,

$$Co + \tfrac{2}{3}\,O_2 \rightarrow \tfrac{1}{3}\,Co_3O_4; \qquad [1]$$

—reaction of Co_3O_4 with Li_2CO_3 to get $LiCoO_2$,

$$\tfrac{1}{3}\,Co_3O_4 + \tfrac{1}{2}\,Li_2CO_3 + \tfrac{1}{12}\,O_2 \rightarrow LiCoO_2 + \tfrac{1}{2}\,CO_2. \qquad [2]$$

Reaction [1] takes place with a weight increase, while reaction [2] occurs with a weight decrease. At the beginning of the process, Co oxidation prevailed over $LiCoO_2$ synthesis; then, above T_{max}, $LiCoO_2$ formation prevailed.

Assuming that Co oxidation rate is independent of the presence of Li_2CO_3, we have calculated the amount of $LiCoO_2$ synthesized at $T < T_{max}$. From thermogravimetric measurement of pure Co at $T = T_{max}$ the fractions of oxidized Co were β = 0.75 (green A) and β = 0.67

TABLE 2
Composition and Cell Parameters of Samples after Thermal Treatment at Various Temperatures

Temperature (°C)	Phases	Green A			Green B		
		a (Å)	c (Å)	c/a	a (Å)	c (Å)	c/a
850	$LiCoO_2$	2.8107(5)	13.971(4)	4.97	2.8072(6)	14.039(7)	5.00
900	$LiCoO_2$	2.8106(3)	13.994(6)	4.98	2.8067(6)	14.034(3)	5.00
950	$LiCoO_2$	2.8158(5)	13.962(7)	4.96	2.8051(2)	14.094(8)	5.02
	Co_3O_4	8.079(2)			8.080(6)		
1000	$LiCoO_2$	2.8107(5)	13.971(2)	4.97			
	Co_3O_4	8.069(5)					
1050	$LiCoO_2$				2.8073(2)	14.136(5)	5.03
	Co_3O_4				8.078(9)		
	$Li_xCo_{1-x}O$				4.235(3)		
1100	$LiCoO_2$	2.8140(3)	13.977(8)	4.97	2.8136(3)	14.092(7)	5.01
	Co_3O_4	8.076(2)			8.071(4)		
	$Li_xCo_{1-x}O$	4.224(5)			4.229(3)		

(green B). For Co/Li_2CO_3 mixtures, at T_{max} Co_3O_4/Co and $LiCoO_2/Co$ molar ratios were $\beta(1 - \phi)/3$ and $\beta\phi$, respectively, where ϕ is the molar fraction of Co_3O_4 formed at $T < T_{max}$ which reacts with Li_2CO_3. We have

$$\beta(1 - \phi)\ (Co + \tfrac{2}{3}\ O_2 \rightarrow \tfrac{1}{3}\ Co_3O_4) \qquad [3]$$

and, writing the sum of reactions [1] and [2],

$$\beta\phi\ (Co + \tfrac{1}{2}\ Li_2CO_3 + \tfrac{3}{4}\ O_2 \rightarrow LiCoO_2 + \tfrac{1}{2}\ CO_2). \qquad [4]$$

From reactions [3] and [4], at T_{max} the relationship between weight change Dm/m_g and ϕ is

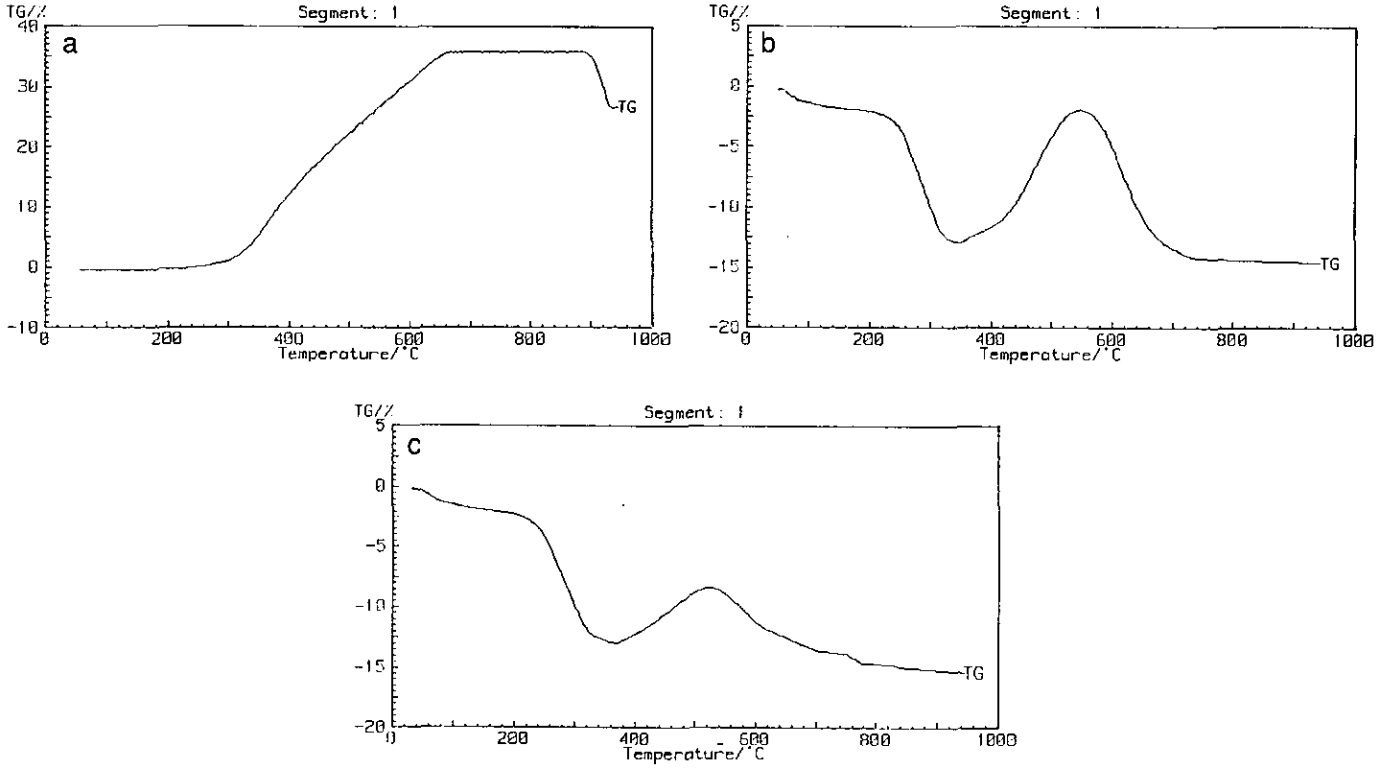

FIG. 4. Thermogravimetric measurements in the dynamic step performed on pure cobalt powder (a), on green A (b) and green B (c).

$$Dm/m_g = \beta(\tfrac{2}{3} M_{O_2} - \phi(\tfrac{1}{2} M_{CO_2} - \tfrac{1}{12} M_{O_2}))/(M_{Co} + z M_{Li_2CO_3}), \quad [5]$$

where M_{Co}, M_{O_2}, M_{CO_2}, and $M_{Li_2CO_3}$ are the molecular weights of related compounds and z is the Li_2Co_3 to Co molar ratio.

From relation [5], if Dm/m_g is known from thermogravimetric measurements, we can obtain ϕ. For green A, $\phi = 0.22$, while for green B, $\phi = 0.55$. Thus, $LiCoO_2$/Co molar ratios $\beta\phi$ were 0.17 and 0.47, respectively; at $T < T_{max}$ for green B the amount of $LiCoO_2$ formed was about three times as high as that for green A. The homogeneity of the green B promotes the reaction of Co_3O_4 with Li_2CO_3 at low temperature. This can explain the formation of nonstoichiometric lithium cobalt oxide from green B at low temperatures (12), notwithstanding lithium excess in the starting mixture.

Stability

To evaluate the stability of $LiCoO_2$ we have measured the weight change by thermogravimetric measurements and investigated the presence of phases unlike $LiCoO_2$ by examining the X-ray diffraction patterns of samples following isothermal treatment in the temperature range 850 to 1100°C.

At 850° no weight loss was revealed by thermogravimetric measurements; as shown in Figs. 2 and 3 and Table 2, diffractometric measurements indicated the formation of single-phase lithium cobalt oxide. For temperatures higher than 850°C thermogravimetric measurements indicated a weight loss of the samples, which increased with increasing temperature. The weight loss is attributable to the evaporation of lithium oxide and oxygen from lithium cobalt oxide, which takes place with the formation of nonstoichiometric lithium cobalt oxide $Li_yCo_{2-y}O_2$ ($y < 1$) by the reaction

$$LiCoO_2 \rightarrow 1/(2 - y)\ Li_yCo_{2-y}O_2 + \varnothing\ Li_2O + \varnothing/2\ O_2, \quad [6]$$

where $\varnothing = (1 - y)/(2 - y)$ is the amount of lithium oxide evaporated as the $Li_2O/LiCoO_2$ molar ratio.

X-ray diffraction patterns of samples from green A and green B following thermal treatment in a furnace at temperatures higher than 900°C showed the presence of Co_3O_4 peaks, related to the formation of CoO. $LiyCo_{2-y}O_2$ is thermally unstable, and during the cooling phase CoO separates from $Li_yCo_{2-y}O_2$,

$$Li_yCo_{2-y}O_2 \rightarrow y\ LiCoO_2 + 2(1 - y)\ CoO. \quad [7]$$

During the cooling of the samples, CoO is transformed to Co_3O_4.

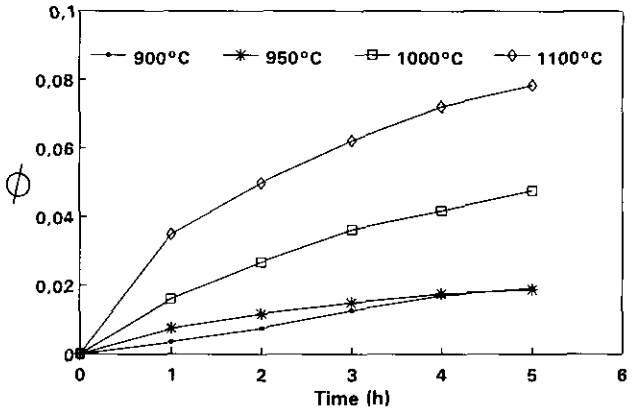

FIG. 5. Dependence on evaporated lithium oxide amount ∅ on isothermal time at different temperatures.

Unlike samples thermally treated in a furnace, X-ray diffraction patterns of samples from green A following thermogravimetric measurements showed no Co_3O_4 at temperatures up to 1000°C. At $T > 1000$°C Co_3O_4 peaks appeared in X-ray diffraction patterns of these samples. This behavior can be explained by the different stabilities of $Li_yCo_{2-y}O_2$ depending on whether the sample is in the form of powder (thermogravimetric measurements) or plaque (thermal treatment in a furnace); the interparticle transfer of matter from the grain boundary between particles following the sintering process, which takes place in plaque samples, could support the reaction of CoO formation at lower temperature.

From thermogravimetric measurements of sample mass at the beginning of the isothermal step (m_{t_0}) and following t hours of isothermal treatment (m_t), we calculated $(m_t - m_{t_0})/m_{t_0} = Dm/m_{t_0}$; then we calculated ∅ as

$$\varnothing = Dm/m_{t_0}\ M_{Li_yCo_{2-y}O_2}/(M_{Li_2O} + \tfrac{1}{2} M_{O_2}), \quad [8]$$

where $M_{Li_yCo_{2-y}O_2}$, with $y = 1$ for green A samples and $y = 0.93$ for green B samples, M_{Li_2O}, and M_{O_2} are the molecular weights of related compounds. Figure 5 shows the dependence of ∅ on isothermal time at different temperatures. Evaporation kinetics is generally expressed as a function of time by

$$\varnothing = kt^n, \quad [9]$$

where t is decomposition time, and k and n are constants. The exponent n is related to the reaction mechanism. Decomposition-controlled evaporation is described by $n = 1$, while diffusion-controlled evaporation is described by $n = 0.5$ to 0.8 (13, 14). Figure 6 shows the log–log plots for Li_2O evaporation in the temperature range 900 to 1100°C. At $T = 900$°C the value $n = 1$ is explained by considering that Li_2O evaporation takes place on the

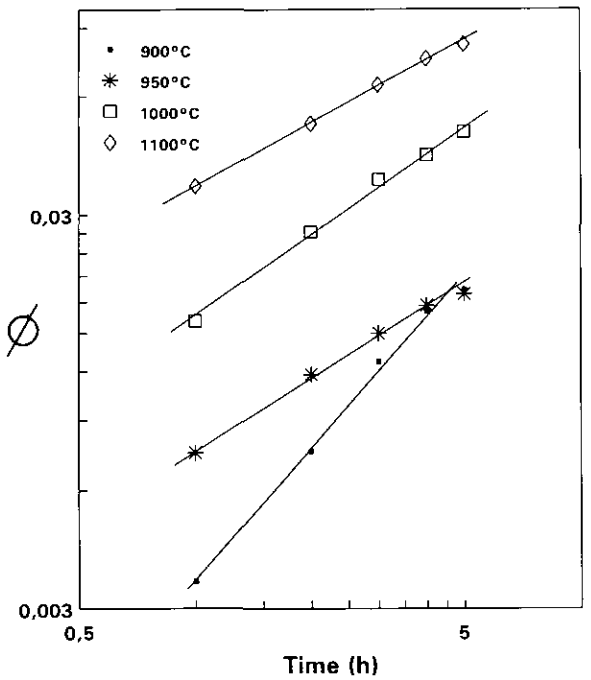

FIG. 6. Log–log plots for lithium oxide evaporation of Fig. 5.

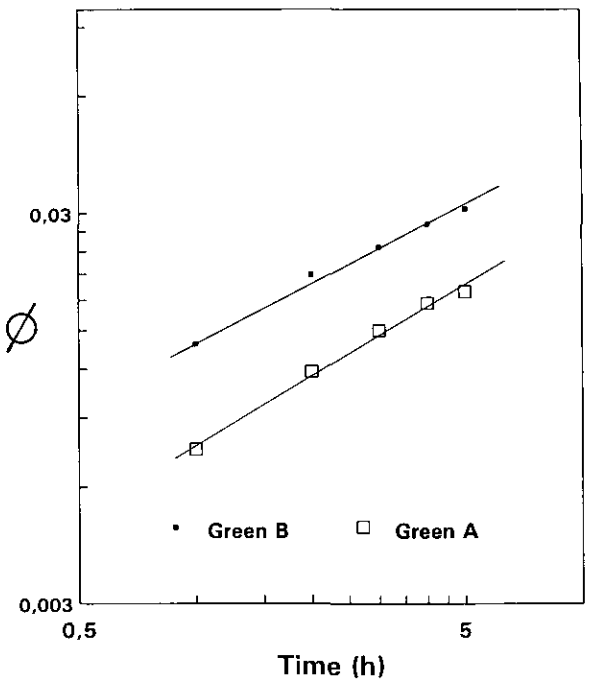

FIG. 8. Log–log plot for lithium oxide evaporation of Fig. 7.

grain surface, so the mechanism is decomposition-controlled. For $T > 900$°C the linear relations in Figure 6 are represented by $n = 0.5$ to 0.7, which indicates that the present evaporation is governed by the diffusion of lithium ions in $Li_yCo_{2-y}O_2$ and through the layer of cobalt oxide surrounding the particles. The estimated error on n was $\pm$ 0.05.

To evaluate the effect on stability of the different temperatures of formation of lithium cobalt oxide from green A and green B, we compared thermogravimetric measurements at 950°C for both samples. Figure 7 shows the dependence of $\varnothing$ on isothermal time at 950°C for green A and green B. Figure 8 shows the log–log plot for Li_2O evaporation from green A and green B. In both cases, Li_2O evaporation was diffusion-controlled, but the evaporation rate was higher for green B; moreover, in confirmation of this, X-ray diffraction patterns showed that the intensity ratio between the main reflection peaks of Co_3O_4 and $LiCoO_2$ of the green B sample was higher than that of the green A sample. Neutron diffraction analysis of $LiCoO_2$ synthesized at low temperature (12) has shown that the cation distribution is $(Li_{0.94}Co_{0.06})_{3a}(Li_{0.04}Co_{0.96})_{3b}O_2$, in which 6% of the cobalt ions are situated in the lithium layer. This analysis also showed that the sample was very slightly deficient in lithium and had the overall stoichiometry $Li_{0.98}Co_{1.02}O_2$. Work on samples of $Li_yNi_{1-y}O_2$ showed substantial cation mixing for $y < 1$ (15). Such mixing of Li into Co sites and Co into Li sites, which we suppose to take place in the crystal lattice of lithium cobalt oxide from green B, increases the energy content of the crystal structure with respect to stoichiometric $LiCoO_2$ and, as a result, decreases its thermal stability. This is confirmed by comparing the c crystallographic parameter of $LiCoO_2$ from green A and green B (see Table 2): the c values of $LiCoO_2$ from green B were higher than those of $LiCoO_2$ from green A, indicating the loss of lattice cohesion of $LiCoO_2$ from green B.

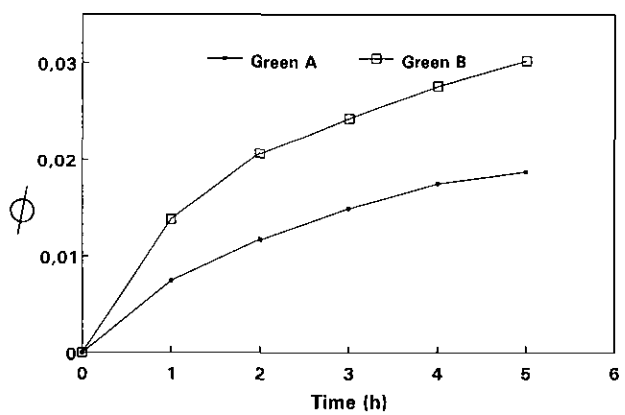

FIG. 7. Dependence of evaporated lithium oxide amount $\varnothing$ on isothermal time at 950°C for samples from green A and green B.

In the X-ray diffraction patterns of samples thermally treated in a furnace at $T > 1000$°C, as shown in Figs. 2 and 3, we can note the presence of peaks of CoO shifted toward high angles; such a shift is due to the decrease in the lattice constant caused by the substitution of Li atoms for Co atoms in the CoO lattice (16), with the formation of a solid solution of the type $Li_xCo_{1-x}O$. During the diffusion in cobalt oxide, some of lithium ions were "cap-

tured'' by CoO to form $Li_xCo_{1-x}O$ solid solution, as

$$x/2\ Li_2O + (1 - x)\ CoO + x/4\ O_2 \rightarrow Li_xCo_{1-x}O. \quad [10]$$

CONCLUSIONS

Thermal treatment in air of a mixture of Co and Li_2CO_3 powder in the proper amounts gave rise to the formation of $LiCoO_2$.

At temperatures higher than 850°C, $LiCoO_2$ decomposition took place by the evaporation of lithium oxide and oxygen and the formation of cobalt oxide. At $T > 1000$°C the formation of $Li_xCo_{1-x}O$ solid solution was also revealed. At 900°C the reaction was decomposition-controlled, while at $T > 900$°C it was diffusion-controlled by lithium diffusion in $Li_yCo_{2-y}O_2$ and CoO solid phases. Moreover, decomposition temperature seemed to depend on formation temperature of lithium cobalt oxide.

REFERENCES

1. H. J. Orman and P. J. Wiseman, *Acta Crystallogr. Sect. C* **40,** 12 (1984).
2. L. D. Dyer, B. S. Borie, Jr., and G. P. Smith, *J. Am. Chem. Soc.* **76,** 1499 (1954).
3. K. Mizushima, P. C. Jones, P. J. Wiseman, and J. B. Goodenough, *Mater. Res. Bull.* **15,** 783 (1980).
4. T. Nagaura and K. Tozawa, *Prog. Batteries Solar Cells* **9,** 209 (1990).
5. J. B. J. Veldhuis, F. C. Eckes, and L. Plomp, *J. Electrochem. Soc.* **139,** L6 (1992).
6. L. Plomp, J. B. J. Veldhuis, E. F. Sitters, and S. B. van der Molen, *J. Power Sources* **39,** 369 (1992).
7. C. Delmas, I. Saadoune, and A. Rougier, *J. Power Sources* **43–44,** 595 (1993).
8. J. N. Riemers and J. R. Dahn, *J. Electrochem. Soc.* **139,** 2091 (1992).
9. J. Bludska, J. Vondrak, P. Stopka, and I. Jakubec, *J. Power Sources* **39,** 313 (1992).
10. E. F. Sitters and L. Plomp, European Patent Appl. 91202194, 1992.
11. M. Antaya, J. R. Dahn, J. S. Preston, E. Rossen, and J. N. Riemers, *J. Electrochem. Soc.* **140,** 575 (1993).
12. R. J. Gummow and M. M. Tackeray, *Solid State Ionics* **53–56,** 681 (1992).
13. T. Sata and Y. Uchida, *Yogyo Kyokaishi* **79,** 110 (1971).
14. T. Sata and T. Yokoyama, *Yogyo Kyokaishi* **81,** 170 (1973).
15. J. R. Dahn, U. Von Sacken, and C. A. Michal, *Solid State Ionics* **44,** 87 (1990).
16. T. Sato, C. Hsien-Chang, T. Endo, and M. Shimada, *J. Mater. Sci. Lett.* **5,** 552 (1986).